Mansoura Engineering Journal

Volume 47 | Issue 3 Article 3

8-2-2022

Coseismic Deformation and Damage Map of the 2022 Afghanistan Earthquakes using SAR Interferometry

Tamer ElGharbawi
Assistant Professor at Civil Engineering DEPT. Faculty of Engineering- Suez Canal University,
tgh@eng.suez.edu.eg

Recommended Citation

ElGharbawi, Tamer (2022) "Coseismic Deformation and Damage Map of the 2022 Afghanistan Earthquakes using SAR Interferometry," *Mansoura Engineering Journal*: Vol. 47 : Iss. 3 , Article 3.
Available at: https://doi.org/10.21608/bfemu.2022.252493

Mansoura University
Faculty of Engineering
Mansoura Engineering Journal

Coseismic Deformation and Damage Map of the 2022 Afghanistan Earthquakes using SAR Interferometry

Tamer ElGharbawi

KEYWORDS
InSAR, Sentinel-1, Coherence, Land Deformation Measurement.

***Abstract* — This paper presents our analysis of the 2022 Afghanistan earthquakes with moment magnitudes of M4.9 and M5.3 that occurred on January 17th, 2022. We used Sentinel-1 data and the interferometric synthetic aperture radar (InSAR) technique to estimate crustal deformation and map the damaged regions. These earthquakes have caused many human casualties and urban destruction. We present our analysis technique that utilizes state-of-the-art cloud processing and correction services in hazard estimation and management. The estimated crustal deformation caused by these earthquakes shows surface deformation values ranging from -16 cm to +7 cm. Moreover, we identified the damaged regions using the phase coherence difference technique. The damaged regions are mainly in rough terrain regions, which indicates the high risk of a rockslide in our study region. We utilize online services for the cloud processing of InSAR data and analysis, also, we used an online service for tropospheric delay correction which shows high reliability for the frequent need for InSAR processing which is required to establish a valid system for continuous monitoring and assessing the natural hazards such as earthquakes.**

I.INTRODUCTION

The Northeastern part of Afghanistan was struck by two earthquakes on January 17, 2022, at 09:35 and 11:40 Universal Time Coordinated (UTC) with moment magnitudes of M4.9 and M5.3, respectively, causing the death of 27 people and 49 injured, in addition to the destruction of hundreds of homes [1] [2] [3]. The stricken region is located in a remote and mountainous area with a high risk of rockslides. The same region was struck by an earthquake with a moment magnitude of M7.5 on October 26, 2015, causing the death of 300 people [4]. These events raised the need to study the destructive damages of such earthquakes to identify the vulnerable regions against rockslide hazards to provide a safer environment for the people inhabiting these remote regions.

Interferometric Synthetic Aperture Radar (InSAR) technique has been used successfully to study surface deformation due to several phenomena such as glacier movements [5], earthquakes [6] [7] [8], and land subsidence [9]. However, InSAR has some drawbacks. For example, tropospheric and ionospheric delays have a significant impact on InSAR observations; InSAR is also affected by the accuracy of the satellites' orbital data. Moreover, the values of crustal deformation obtained from InSAR are subjected to errors in phase unwrapping and present relative deformation values.

To mitigate tropospheric delay effects presented in InSAR [10] and [11] have incorporated GPS based Zenithal Tropospheric Delay (ZTD) with a topography based turbulence

Received: (12 April, 2022) - Revised: (03 June, 2022) - Accepted: (14 June, 2022)

Corresponding Author: *Tamer ElGharbawi, Assistant Professor at Civil Engineering DEPT. Faculty of Engineering- Suez Canal University (emails: tgh@eng.suez.edu.eg - tamer_ib@yahoo.com)*

(Ser. NO. BFEMU-2204-1251)

model, [12] used an exponential altitude-based model estimated from GPS ZTD, [7] and [13] used ZTD estimated from the continuous GPS network and kriging algorithm for correcting the tropospheric delay at Tokyo area, Japan. [14] used a bilinear algorithm to remove baseline errors applied on interferograms and a nonlinear algorithm applied after phase unwrapping. [15] used GPS velocities to correct baseline errors by removing a linear ramp from an interferometric stack in San Andreas fault.

To identify damaged regions, the coherent change detection technique (CCD) was proposed, which relies on the interferometric phase decorrelation rate of the radar signals observed before and after the earthquake. Many researchers applied CCD techniques to detect disasters' related damages like earthquakes [16], floods [17], soil liquefaction [18], industrial explosions [19], and volcanos [20]. [21] presented the relation between InSAR phase decorrelation and the severity of damages using the difference between pre- and post-event coherence maps. [22] used a coherence-based change index to identify the urban damage resulted from the Bam earthquake.

This paper utilizes InSAR technique and Sentinel-1 SAR images to estimate the crustal deformations caused by the 2022 Afghanistan earthquakes and map the damaged regions to identify the hazardous areas. We used Sentinel-1 SAR images to create coseismic and preseismic interferograms. Because the GPS stations are not available in our study region, we used the Generic Atmospheric Correction Online Service for InSAR (GACOS) [23] to remove the tropospheric artifact in the generated interferograms. The ionospheric artifact was neglected because Sentinel-1 uses a C-band signal which is hardly affected by ionospheric activity. The estimated crustal deformation shows a slide motion that is consistent with the existing faults map of the region. Moreover, we used the coherence difference methodology [18] [19] to estimate and map damaged regions.

This paper is organized as follows, Section 2 presents the study area and dataset, section 3 describes the analysis methodology, section 4 presents the application results of the Afghanistan Northern region and finally, section 5 is dedicated to conclusions.

II. Study Area and Dataset

A. Study Area

This paper focuses on the Northeastern part of Afghanistan near the city of Qala i Naw (Figure 1), which was unfortunate to endure the devastating damages of the two earthquakes that struck Afghanistan on January 17, 2022. The first earthquake occurred at 09:35 UTC with a moment magnitude of M4.9, its epicenter location was at 63.667˚ East and 34.936˚ North, and a depth of 10 km [2]. The second earthquake occurred nearly two hours later at 11:40 UTC with a moment magnitude of M5.3, its epicenter location was at 63.621˚ East and 34.929˚ North and a depth of 11.4 km [3]. In Figure 1. b the locations of the epicenters are shown in addition to the seismic fault lines in the study region acquired from the U.S. Geological Survey [24].

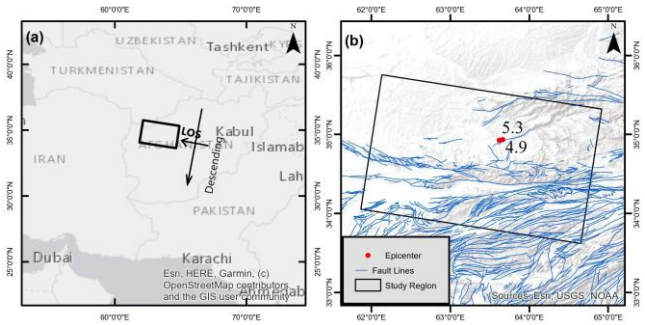

Figure 1. (a) Location of study region within Afghanistan (black rectangle), (b) Study area with SAR image coverage and the epicenters of the earthquakes under study (red dots), and the faults lines map (blue lines) [24]. Base map provided by (© Esri) [25]

B. Dataset

We utilize Copernicus Sentinel-1 data 2022, provided by the European Space Agency (ESA). Three Sentinel 1-A, C-band Interferometric Wide swath SAR images were acquired using polarization of Vertical – Vertical (VV) mode in descending direction (Figure 1.b). We use single look complex (SLC) images with multi-looking of 4-by-20 pixels in the azimuth and range directions, respectively. The final products were geocoded using Copernicus Digital Elevation Model (DEM) 30m resolution (GLO-30) [26] and resampled to 80 m by 80 m pixel size in Universal Transverse Mercator (UTM) zone 41 N.

We use the acquired images to create three interferograms and their corresponding coherence maps (Table 1). This interferometric stack formation ensures more accurate change detection results by enabling us to isolate the pixels' behavior before and after the event.

TABLE 1
DETAILS OF SAR IMAGES

No.	Master	Slave	$B_{\perp}$ (m.)	ΔT (DAYS)	Figures	Satellite Signal Direction
1	5 Jan. 2022	17 Jan. 2022	-9.93	12	Figure 3.a	Sentinel 1-A (C-band) (VV) Descending
2	5 Jan. 2022	29 Jan. 2022	-46.63	24	Figure 3.b	
3	17 Jan. 2022	29 Jan. 2022	-36.71	12	Figures 2.a, 2.b	

III. Methodology

This paper presents the analysis and estimation of crustal deformation induced by the 2022 Afghanistan earthquakes that occurred on January 17, 2022. (1) presents the interferometric phase generated by complex conjugating two SAR single look complex (SLC) images. The interferometric phase contains topographic effects ϕ_{Topo} which is removed using the Copernicus GLO-30 DEM. The interferometric phase also contains surface deformation $\phi_{Deform.}$, tropospheric effects ϕ_{Tropo}, ionospheric effects ϕ_{Iono}, baseline error $\phi_{Baseline}$ and noise ϕ_{Noise}.

$$\phi_{InSAR} = \phi_{Topo} + \phi_{Deform.} + \phi_{Tropo} + \phi_{Iono} + \phi_{Baseline} + \phi_{Noise} \quad (1)$$

Tropospheric delay is highly variable, and it affects the whole deformation map, as well as causes extra local disturbances, depending on a variety of factors including altitude, water vapor, temperature, and wind. The ionospheric effect is mainly dependent on solar activity and the radio wave's inverse squared frequency; therefore, its effect can be neglected when using radio waves with high frequency like the C-band used in Sentinel-1, according to (2).

$$\tau_{phase} = -\frac{2K_0 STEC}{f^2} \text{ [m]} \quad (2)$$

Where the constant K_0 equals 40.28 m^3s^{-2} and STEC is the Slant range Total Electron Content (TEC). The TEC refers to the density of atmospheric free electrons in a unit area cylinder in the direction of nadir. The STEC is proportional to TEC by $(1/\cos z)$, where z is the zenith angle [27].

Complex interferograms were generated as shown in (Table 1), flattened using DEM, filtered, and phase unwrapped using Minimum Cost Flow (MCF). Moreover, the phase coherence was estimated for each interferogram. It should be noted that because of the small normal baseline and the accurate orbital data obtained the effect of baseline error was minimal in our processed scenes; therefore, the baseline error was neglected in the processed unwrapped phase. The unwrapped phase was converted to displacements using.

$$\Delta = -1 * \frac{\phi \times \lambda}{4\pi} \quad (3)$$

Where λ is the wavelength and ϕ is the unwrapped phase. All InSAR products were processed by ASF DAAC HyP3 2022 using the hyp3_gamma plugin version 5.2.0 running GAMMA release 20210701 [28].

A. *Tropospheric Correction*

The process of tropospheric correction is to calculate the tropospheric delay difference map for the InSAR unwrapped phase. We use the Generic Atmospheric Correction Online Service for InSAR (GACOS) [23] to estimate the tropospheric delay at the observation times of the master and slave images for each interferometric pair and by differencing the two maps (4)., the tropospheric delay can be estimated and used to correct the generated interferograms.

$$d\,ZTD_{InSAR} = ZTD^{Day2} - ZTD^{Day1} \quad (4)$$

GACOS employs the Iterative Tropospheric Decomposition (ITD) model to separate stratified and turbulent signals from tropospheric total delays and provide high spatial resolution zenith total delay maps for use in InSAR correction and other applications. GACOS offers the following essential features: (i) global availability; (ii) near real-time operation; and (iii) ease of implementation.

B. *Coherence Estimation*

Interferometric phase coherence is a measure of how comparable two acquisitions' interferometric SAR returns are. The amount of the estimated coherence reflects how much the target has changed between the acquisition times of the SAR images. (5) is used to calculate the complex phase coherence (γ) [29].

$$\gamma = \frac{E\langle s_1 \cdot s_2^* \rangle}{\sqrt{E\langle |s_1|^2 \rangle \cdot E\langle |s_2|^2 \rangle}} \quad (5)$$

Where s_1 and s_2 are the coregistered SAR images complex signal, * is the operator of the complex conjugate, $|\cdot|$ is the absolute operator and $E\langle\cdot\rangle$ is the mathematical expectation. Practically, estimating the mathematical expectation of radar signals is not feasible, therefore the ensembled average of coherence $(\hat{\gamma})$ is calculated by averaging signals over a moving window with the assumption of uncorrelated noise and signal (6) [30] [29].

$$\hat{\gamma} = \frac{\left|\sum_{i=1}^{N} s_{1i} \cdot s_{2i}^* \cdot e^{j\phi(i)}\right|}{\sqrt{\sum_{i=1}^{N} |s_{1i}|^2 \cdot \sum_{i=1}^{N} |s_{2i}|^2}} \quad (6)$$

Where i is the i^{th} pixel in the moving averaging window with a total number of N pixels. The coherence value $\hat{\gamma}$ is biased because of the correlated portion of the signal $\phi(i)$ in the InSAR phase. This portion of the InSAR phase contains topography, motion, and viewing geometry effects. The phase decorrelation effects are illustrated by [29] which decomposed the decorrelation sources as in (7).

$$\gamma_{total} = \gamma_{temporal} \cdot \gamma_{spatial} \cdot \gamma_{thermal} \quad (7)$$

Where $\gamma_{temporal}$ is the estimate of physical changes of the pixels' phase between acquisitions, $\gamma_{spatial}$ is related to the geometric relations between the acquisitions and $\gamma_{thermal}$ is related to the radar thermal noise.

IV. APPLICATION

A. *Crustal Deformation*

We created a coseismic interferogram using the Sentinel-1 images that were acquired on January 17th and January 29th, 2022 (Table 1) using Alaska Satellite Facility Vertix service [28]. The interferogram was flattened using Copernicus GLO-30 DEM, unwrapped using MCF, and geocoded with a spatial resolution of 80 m by 80 m. Figure 2.a shows the coseismic interferogram with wrapped phase from -π to π, the fringes suggest deformation in a slip mode which is consistent with the fault lines [24] shown in Figure 1.b. The estimated coseismic coherence is presented in Figure 2.b and shows high coherence in many regions and other heavily decorrelated regions which correspond to the surface changes in rough terrain regions that can be attributed to the occurrence of rockslides.

We estimated the tropospheric delay at the time of SAR image acquisition using [23] and estimated the tropospheric delay difference using (4) Figure 2. c. The estimated tropospheric delay was used to correct the unwrapped interferometric phase before converting the phase to meters using (3). Because of the arid nature of our study regions, we can see that the tropospheric delay has a small variation ranging from -3 cm to + 3 cm.

The final Line of Sight (LOS) deformation map is presented in Figure 2.4 which shows the crustal deformation induced by the earthquakes in meters after applying phase unwrapping and corrections. The deformation ranges from -0.15 m to +0.07 m and a clear slide deformation is present in the deformation map which is consistent with the seismic fault lines of the regions [24]. The slide directions are shown as black arrows in Figure 2.d.

B. Damaged Regions

To estimate damaged regions, we applied the coherence difference method [18]. We estimated a preseismic coherence map (Table 1, No.1) Figure 3.a and a coseismic coherence map (Table 1, No.2) Figure 3.b. Then, we subtracted the preseismic coherence from the coseismic coherence, this approach identifies the pixels that lost phase coherence as a result of the earthquakes. We chose an empirical threshold of <-0.5 [18] for the coherence difference map to distinguish the damaged pixels in our study regions. The damaged regions are shown in Figure 3.c in red color. Most of the damaged regions were located in rough terrain regions which indicated rockslide-related damages as a result of the earthquakes.

V. CONCLUSION

The crustal deformation map of the 2022 Afghanistan earthquakes was presented which shows crustal deformation in the range of -16 cm to +7 cm. The deformation map verifies s slide slip motion along the predefined fault lines in the study region. The damaged regions were identified using the coherence difference technique which shows the vulnerability of our study region against the occurrence of rockslides, especially in rough terrain and high slope regions. The endangered zones are not especially loated near the fault lines, but around the rough topography which increase the chance of rockslide hazard regardless of the amount of permanent crustal motion. We utilized several online InSAR processing services in the data processing of this research which shows the high level of accuracy and reliability of these novel online services.

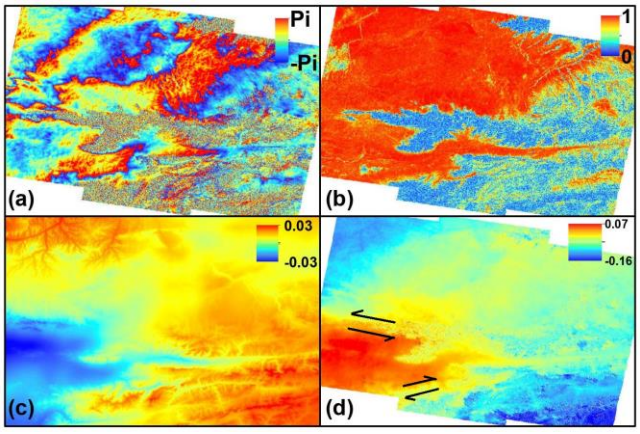

Figure 2. (a) Coseismic interferogram (Table 1, No.3), (b) Estimated Coseismic phase coherence ranging from 0 to 1, (c) Tropospheric delay in meters for coseismic interferogram (Table 1, No.3) (d) The estimated coseismic crustal deformation in meters along the LOS direction, the arrows show slip direction.

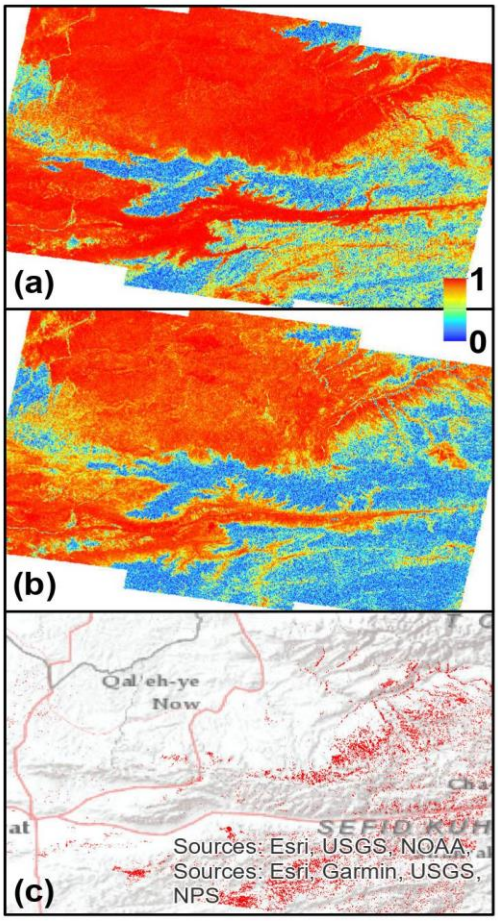

Figure 3. (a) Preseismic phase coherence map (Table 1, No.1), (b) Coeseismic phase coherence map (Table 1, No.2), (c) Estimated damaged region using coherence difference method (red color)

FUNDING STATEMENT:

"The Author receives no financial support for this research, authorship or publication of his article"

DECLARATION OF CONFLICTING INTERESTS STATEMENT:

"No potential conflicts of interest concerning research, authorship or publication of his article"

REFERENCES

[1] D. Zucchino and S. Hassan, "Two Earthquakes Strike Afghanistan, Killing at Least 27," 18 January 2022. [Online]. Available: https://archive.ph/RSNVr.

[2] "M 4.9 - 49 km E of Qala i Naw, Afghanistan," [Online]. Available: https://earthquake.usgs.gov/earthquakes/eventpage/us7000gcle/executive.

[3] "M 5.3 - 45 km E of Qala i Naw, Afghanistan," [Online]. Available: https://earthquake.usgs.gov/earthquakes/eventpage/us7000gclu/executive.

[4] "M 7.5 - Hindu Kush region, Afghanistan," [Online]. Available: https://earthquake.usgs.gov/earthquakes/eventpage/us10003re5/executive.

[5] R. M. Goldstein, H. Engelhardt, B. Kamb and R. M. Frolich, "Satellite Radar Interferometry for Monitoring Ice Sheet Motion: Application to an Antarctic Ice Stream," SCIENCE, vol. VOL.262, pp. 1525-1530, 1993.

[6] D. Massonnet, K. Feigl, R. Marc and F. Adragna, "Radar interferometric mapping of deformation in the year after the Landers earthquake," Nature, vol. VOL. 369, pp. 227-230, 1994.

[7] T. ElGharbawi and M. Tamura, "Measuring deformations using SAR interferometry and GPS observables with geodetic accuracy: Application

to Tokyo, Japan," ISPRS Journal of Photogrammetry and Remote Sensing, vol. 88, pp. 156-165, 2014.
[8] T. ElGharbawi and M. Tamura, "Coseismic and postseismic deformation estimation of the 2011 Tohoku earthquake in Kanto Region, Japan, using InSAR time series analysis and GPS," Remote Sensing of Environment, vol. 168, pp. 374-387, 2015.
[9] S. M. Buckley, P. Rosen, S. Hensley and B. Tapley, "Land subsidence in Houston, Texas, measured by radar interferometry," JOURNAL OF GEOPHYSICAL RESEARCH, vol. VOL. 108, pp. 8-1:8-12, 2003.
[10] Z. Li, E. Fielding, P. Cross and J.-P. Muller, "Interferometric synthetic aperture radar atmospheric correction:GPS topography-dependent turbulence model," JOURNAL OF GEOPHYSICAL RESEARCH, vol. VOL. 110, p. B03410, 2006.
[11] X. Song, D. Li and M. Liao, "REPRODUCTION OF INSAR ATMOSPHERIC SIGNAL USING GPS DATA BASED ON TOPOGRAPHY-DEPENDENT AND TURBULENT MIXING MODEL," in 2008 Dragon Symposium, Dragon 1 Programme, Final Results 2004 (ESA SP-655, April 2008), Beijing, P.R. China, 2008.
[12] F. Onn and H. A. Zebker, "Correction for interferometric synthetic aperture radar atmospheric phase artifacts using time series of zenith wet delay observations from a GPS network," JOURNAL OF GEOPHYSICAL RESEARCH, vol. VOL. 111, p. B09102, 2006.
[13] Janssen, L. Ge and C. Rizos, "Tropospheric Corrections to SAR Interferometry from GPS Observations," GPS Solutions, p. 140–151, 2004.
[14] S. Zhang, T. Li, J. Liu and Y. Xia, "Research on the Linear and Nonlinear Methods of Correcting Baseline Errors on SAR Interferograms," The International Archives of the Photogrammetry, Remote Sensing and Spatial Information Sciences., pp. 161-164, 2008.
[15] Y. Fialko, "Interseismic strain accumulation and the earthquake potential on the southern San Andreas fault system," Nature, vol. VOL.441, pp. 968-971, 2006.
[16] G. Arciniegas, W. Bijker, N. Kerle and V. Tolpekin, "Coherence- and amplitude-based analysis of seismogenic damage in Bam, Iran, using ENVISAT ASAR data," IEEE Transactions on Geoscience and Remote Sensing, vol. 45, no. 6, pp. 1571-1581, 2007.
[17] Y. Li, S. Martinis and M. Wieland, "Urban flood mapping with an active self-learning convolutional neural network based on TerraSAR-X intensity and interferometric coherence," Isprs Journal of Photogrammetry and Remote Sensing, vol. 152, pp. 178-191, 2019.
[18] T. ElGharbawi and M. Tamura, "Estimating deformation due to soil liquefaction in Urayasu city, Japan using permanent scatterers," ISPRS Journal of Photogrammetry and Remote Sensing, vol. 109, pp. 152-164, 2015.
[19] T. ElGharbawi and F. Zarzoura, "Damage detection using SAR coherence statistical analysis, application to Beirut, Lebanon," ISPRS Journal of Photogrammetry and Remote Sensing, vol. 173, pp. 1-9, 2021.
[20] J. Jung, D.-j. Kim, M. Lavalle and S.-H. Yun, "Coherent change detection using InSAR temporal decorrelation model: a case study for volcanic ash detection," IEEE Transactions on Geoscience and Remote Sensing, vol. 54, no. 10, pp. 5765-5775, 2016.
[21] C. Yonezawa and S. Takeuchi, "Decorrelation of SAR data by urban damages caused by the 1995 Hyogoken-nanbu earthquake," International Journal of Remote Sensing, vol. 22, no. 8, pp. 1585-1600, 2001.
[22] J. Hoffmann, "Mapping damage during the Bam (Iran) earthquake using interferometric coherence," Journal of Remote Sensing, vol. 28, no. 6, pp. 1199-1216, 2007.
[23] C. Yu, Z. Li, N. T. Penna and P. Crippa, "Generic atmospheric correction model for interferometric synthetic aperture radar observations," Journal of Geophysical Research: Solid Earth, vol. 103, no. 10, pp. 9202--9222, 2018.
[24] "Geologic Faults of Afghanistan," U.S. Geological Survey, [Online]. Available: https://data.doi.gov/dataset/geologic-faults-of-afghanistan-fltafg. [Accessed 3 4 2022].
[25] Esri,"https://basemaps.arcgis.com/arcgis/rest/services/World_Basemap_v2/VectorTileServer," 2020. [Online].
[26] "CSCDA Portal," Copernicus Space Component Data Access system, [Online]. Available: https://spacedata.copernicus.eu/. [Accessed 5 4 2022].
[27] F. Meyer, R. Bamler, N. Jakowski and T. Fritz, "The Potential of Low-Frequency SAR Systems for Mapping Ionospheric TEC Distributions," IEEE GEOSCIENCE AND REMOTE SENSING LETTERS, pp. 560-564, 2006.
[28] "ASF Data Search Vertex," EARTH DATA, [Online]. Available: https://search.asf.alaska.edu/#/. [Accessed 3 4 2022].
[29] H. Zebker and J. Villasenor, "Decorrelation in interferometric radar echoes," IEEE Transactions on Geoscience and Remote Sensing, vol. 30, no. 5, pp. 950-959, 1992.
[30] H. Zebker and K. Chen, "Accurate estimation of correlation in InSAR observations," IEEE Geoscience and Remote Sensing Letters, vol. 2, no. 2, pp. 124-127, 2005.

Title Arabic:

خريطة التحركات الأرضية والأضرار الناتجة من زلزال أفغانستان ٢٠٢٢
باستخدام الصور الرادارية التداخلية (انترفروجرام)

Arabic Abstract:

يركز هذا البحث على دراسة زلزالي افغانستان ٢٠٢٢ في ١٧ يناير ٢٠٢٢ بقوة ٤,٩ و ٥,٣ بمقياس ريختر و في خلال مدة زمنية مقدارها ساعتان. تم استخدام بيانات القمر الصناعي سنتينال-١ وتقنية الصور الرادارية التداخلية (انترفروجرام) لحساب تحركات القشرة الأرضية ورسم خريطة للمناطق المتضررة. تسببت هذه الزلازل في وقوع العديد من الضحايا البشرية ودمارًا في المناطق الحضرية. تظهر الدراسة مقدار تحركات سطح الارض الناجمة من هذه الزلازل حيث تتراوح من -١٦ سم إلى +٧ سم. علاوة على ذلك، استخدمنا تقنية فرق توافق الطور الموجي للإشارة الرادارية لتحديد المناطق المتضررة بسبب الزلازل. تقع المناطق المتضررة بشكل أساسي في المناطق ذات التضاريس الوعرة مما يشير إلى ارتفاع مخاطر حدوث انزلاق صخري في منطقة الدراسة. تم استخدم الخدمات المتاحة عبر الإنترنت للمعالجة السحابية لبيانات وتحليلات الصور الرادارية، كما استخدمنا خدمة عبر الإنترنت لتصحيح خطأ التروبوسفير والتي تُظهر درجة عالية من الدقة المطلوبة لإنشاء نظام صالح للمراقبة المستمرة وتقييم الأخطار الطبيعية مثل الزلازل.